CHAPTER IV
RESULTS AND DISCUSSION

4.1 Surface Characterization

The surface characterizations were conduced to analyze oxide films which were formed on steel under simulated primary coolant of CANDU reactors for different coolant velocities (5, 10 and 20 m/s). The bare metal probe was investigated as a reference.

4.1.1 SEM/EDX Analysis

The surface morphology of the oxide film was investigated by SEM micrograph. Figure 4.1 shows the overview morphology of the oxide surface at 1,000X magnifications. It is seen that the original metal surface is not smooth, as shown in Figure 4.1a. The oxide film formed under 10 m/s coolant velocity had a rough surface compare with the other velocities.

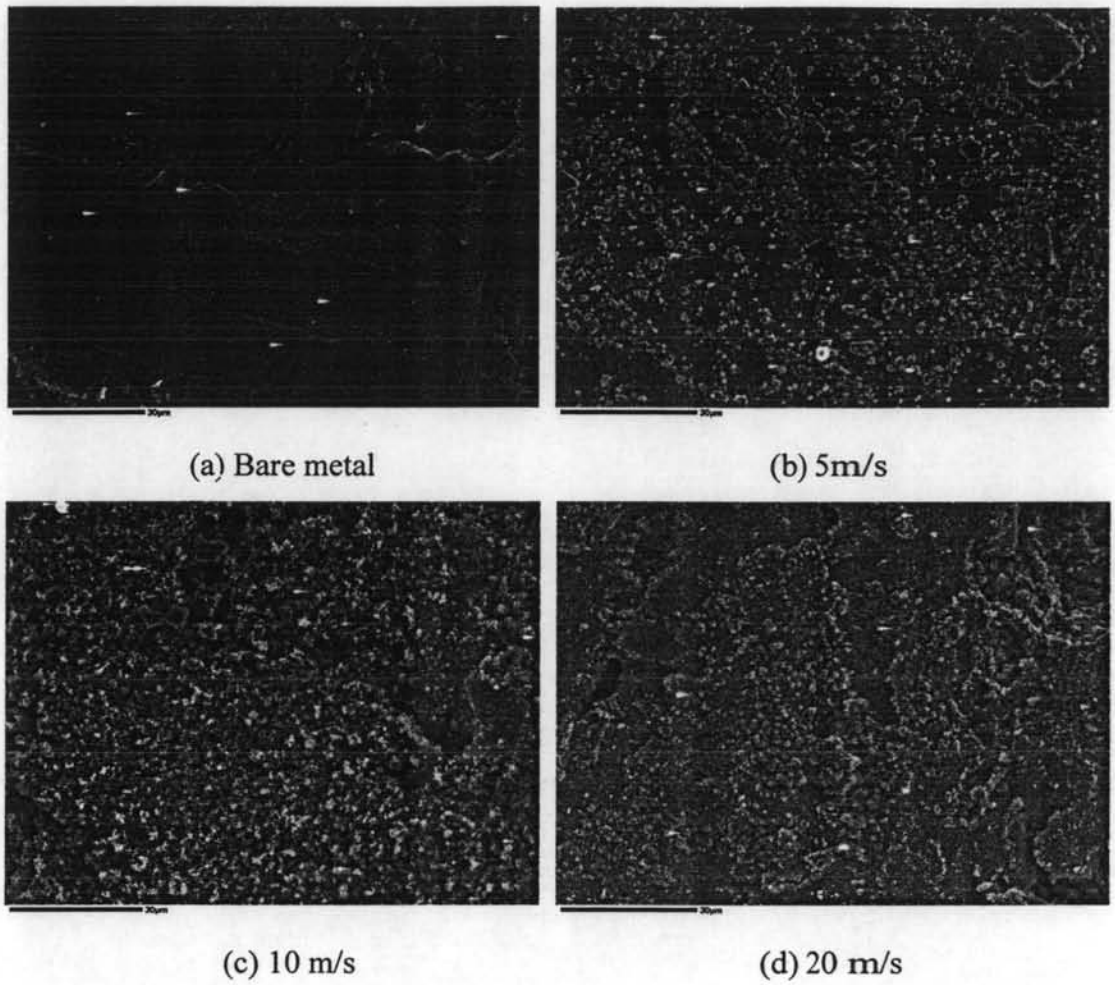

Figure 4.1 SEM micrograph of the oxide surface formed under different coolant velocities at 1,000X magnifications.

Figure 4.2 shows the detailed oxide morphology at higher resolution 10,000X magnifications. Figure 4.2a shows that some oxide could be formed on the metal surface even though this tube has never been used before. However, this original oxide is very thin; less than 1 nm. After each specimen was exposed to different coolant velocities, the oxide layer formed in significantly different structures. Apparently, the oxide consists of large particle (so-call outer oxide) and small particles (so-call inner oxide).

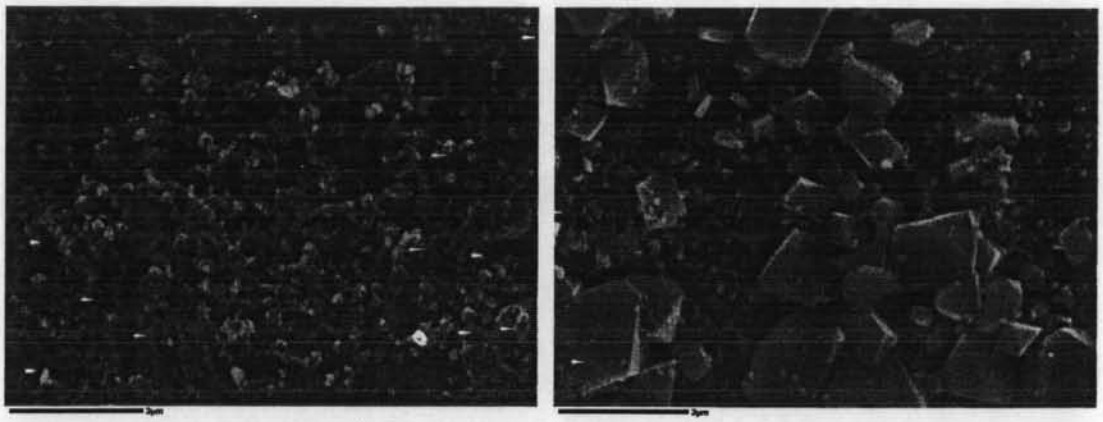

(a) Bare metal (b) 5m/s

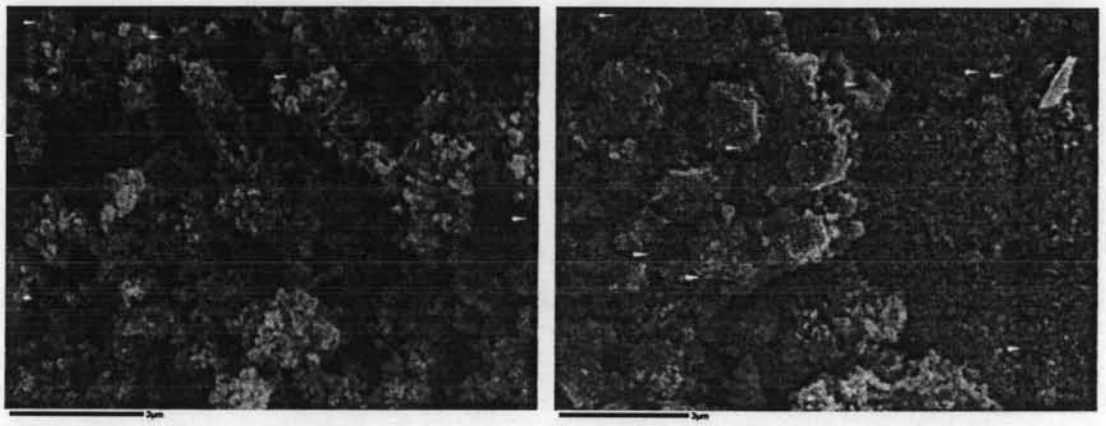

(c) 10 m/s (d) 20 m/s

Figure 4.2 SEM micrograph of the oxide surface formed under different coolant velocities at 10,000X magnifications.

Under a 5 m/s coolant velocity, it is clearly seen that large oxide particles overlay a layer of finer particles. However, the large oxide particles can not be seen on the outer oxide surface of the 10 m/s sample. The surface is rough but only consists of small particles. For the 20 m/s sample, the outer oxide, which exists only in certain areas, consists of both large and small oxide particles. Therefore, it is evident that coolant flow velocity affected the oxide layer characteristics.

Table 4.1 EDX analysis of bare metal and oxide film in different velocities

Atomic %	Bare Metal	5 m/s		10 m/s		20 m/s	
		Small particle	Large Particle	Small Particle	Large particle	Small particle	Large Particle
O	-	50.60	50.15	50.58	-	50.34	50.35
Al	-	-	-	0.24	-	-	-
Si	0.77	0.40	0.09	0.55	-	0.52	0.14
P	-	-	-	0.04	-	-	-
S	-	-	-	0.13	-	-	-
Ca	-	-	-	0.22	-	-	-
Ti	-	0.07	0.22	0.11	-	0.14	0.5
Cr	-	0.02	0.02	0.13	-	0.05	0.16
Mn	0.77	0.28	0.28	0.50	-	0.22	0.11
Fe	98.51	48.63	49.25	47.16	-	46.34	39.73
Ni	-	-	-	0.36	-	2.41	9.02

The chemical compositions of the bare metal probe and oxide film which was formed at different velocities are shown in Table 4.1. It is seen that there were trace contaminations, such as Al, Ca and Ti, present in the oxide, especially in the oxide formed under 10 m/s velocity. The system was contaminated from oil leakage during the experiment. Moreover, high values of Ni contamination in the oxide were found in the 20 m/s velocity sample, especially in the large oxide particles. These chemicals are not in the original composition of the A106B metal. Therefore, these contaminations must have come from some part of the loop components such as the autoclave or the oil.

4.1.2 TEM Analysis

Oxide thickness and its structure were investigated by TEM analysis. All of the TEM specimens were prepared by a "Lift Out" technique. The specimen surface was polished with a Ga^+ ion beam until it reached the desired thickness, 120 to 500 nm.

4.1.2.1 5 m/s Coolant Velocity

Figure 4.3 shows a cross sectional picture of the oxide film formed under 5 m/s coolant velocity. Overviews and detailed pictures of oxide films are shown in Figure 4.3a and 4.3b, respectively. At higher magnifications, it is clear that the oxide forms a duplex layer. The large oxide particles overlie a layer of small particles.

It is generally accepted that the oxide avoids forming near a point or corner on any surface. Therefore, it is not surprising that the oxide formed an uneven layer since the original metal surface is rough, as shown in Figure 4.3b. However, it is possible that the oxide layer may continue to grow if the sample was given longer exposure.

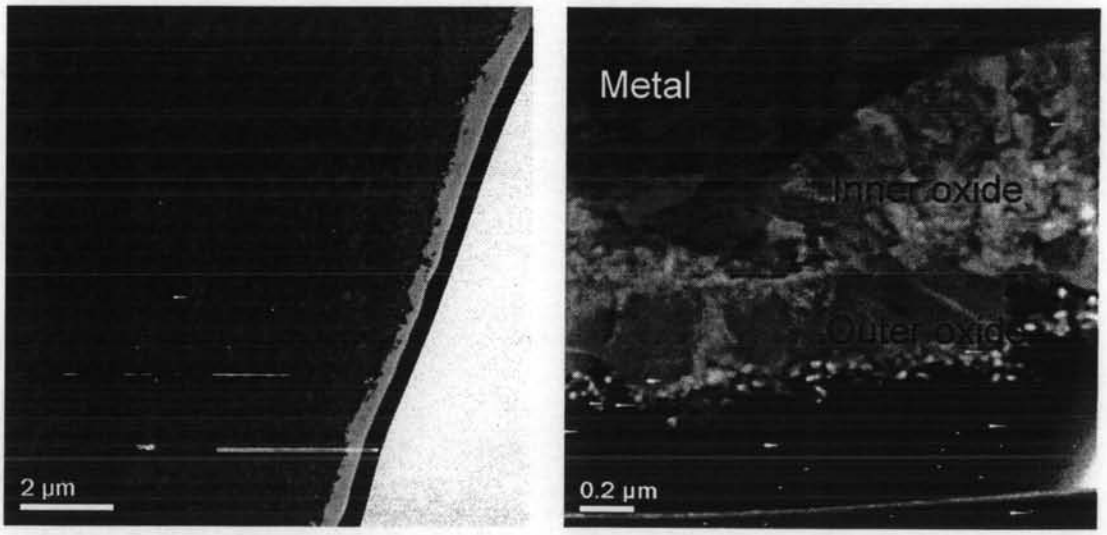

(a) Overview picture of oxide film (b) Oxide film in higher magnifications

Figure 4.3 TEM micrograph of oxide film formed under 5 m/s coolant velocity.

Figure 4.4 shows the chemical composition profile in depth of the oxide film. Scanning was performed in 30 spots along the blue line, as shown in Figure 4.4a, from metal through oxide layer. Since the Fe and O ratio is relatively constant, both the inner and outer oxides have the same structure. The sudden changing in Fe and O concentrations in inner oxide can clearly identify the metal/oxide interface. The dramatically decrease of Fe concentration in the outer oxide shows the end of the oxide layer. Trace of Si, Cr and Mn were also detected by TEM line scanning. They are in the original compositions of A106B steel. However, their concentrations are very low, less than 1%, and believe to unimportant in regard to the oxide structure.

Another method to determine the chemical composition of the oxide film is EDX mapping, as shown in Figure 4.5. The brighter color zone represents the greater element concentration. However, this color level comparison technique can be applied with only the same element. Sharp contrast in the Fe and O map clearly identify the metal/oxide interface. The O map confirmed that the film is an oxide compound. No significant difference in Cr concentration was found in the oxide layer. The Si concentration in outer oxide is less than for the metal and inner oxide.

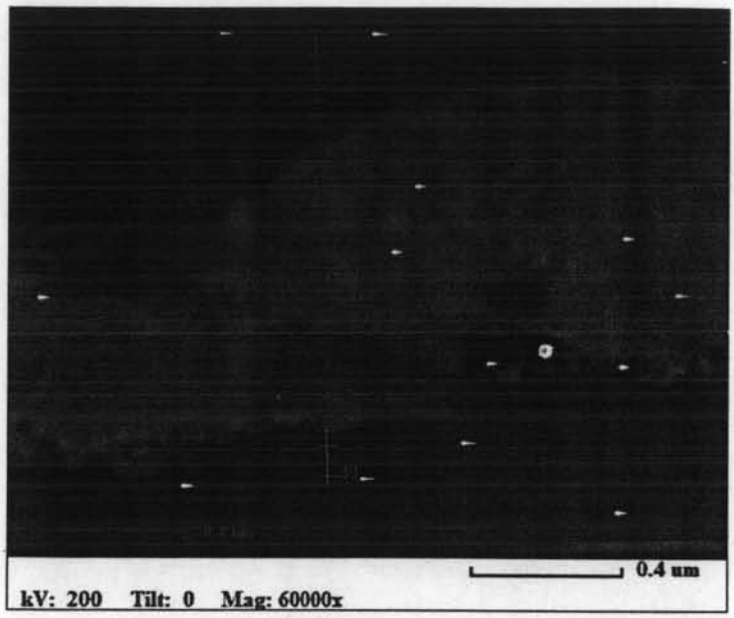

(a)

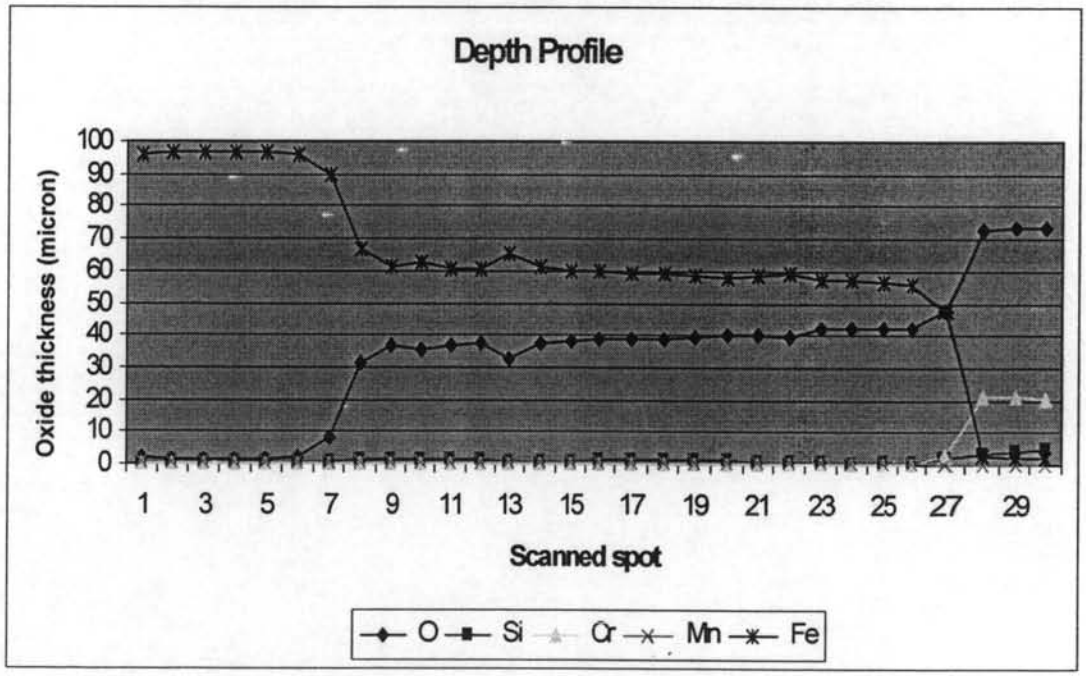

(b)

Figure 4.4 TEM line scanning of oxide film formed under 5 m/s coolant velocity. (a) TEM micrograph with annotated line. (b) Depth profile of oxide film.

(a) Cross sectional micrograph of oxide film

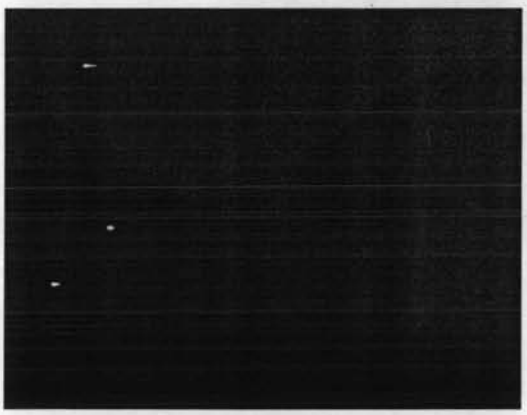

(b) Iron

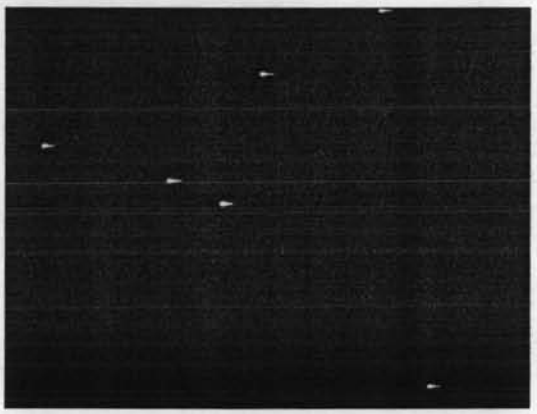

(c) Oxygen

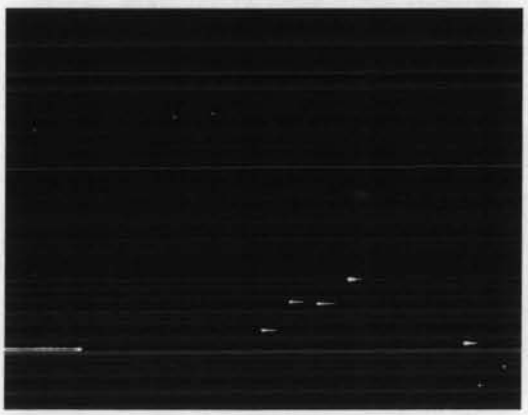

(c) Chromium

(d) Silicon

Figure 4.5 EDX mapping of 5 m/s sample.

a) Inner Layer

The inner oxide layer varied from 0.08 to 0.74 microns. The oxide mainly consists of iron and oxygen, as shown by the depth profile. The maximum concentration of Fe was 67 % at the metal/oxide interface and then gradually decreases toward the outer surface. Oxygen reaches its maximum concentration, 47 %, at the oxide/solution interface and gradually decreases toward the metal/oxide interface. However, the oxygen concentration may not be reliable. The copper peak can overlap with the oxygen peak in EDX spectrum. Since the TEM sample carrier is made of copper, the oxygen concentration calculation might be affected by copper content in the system.

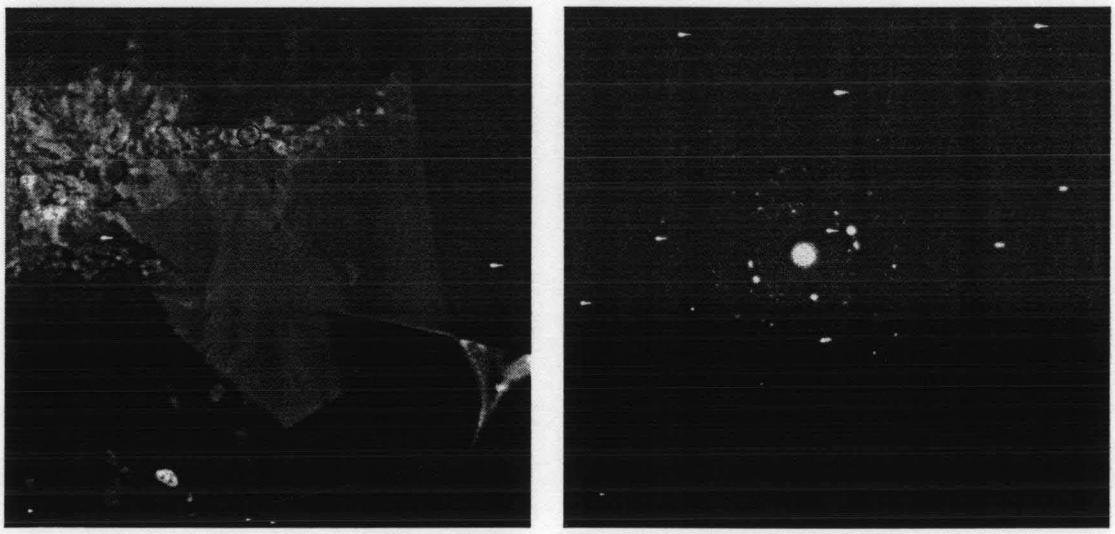

(a) (b)

Figure 4.6 TEM micrograph of inner oxide layer, which developed under 5 m/s coolant velocity, with its electron diffraction pattern.
(a) TEM micrograph of selected area in inner oxide layer. (b) Diffraction pattern of circular area.

Table 4.2 d-spacing value and reflection plane indices (h, k, l) of Fe_3O_4

d-spacing	0.485	0.298	0.254	0.243	0.209	0.171	0.148	0.160
(h, k, l)	1 1 1	2 2 0	3 1 1	2 2 2	4 0 0	4 2 2	4 4 0	5 1 1

A selected area of the inner oxide layer was analyzed by the electron diffraction pattern, as shown in Figure 4.6a. The d-spacing values of the spotty ring in the electron diffraction pattern can be used to identify the crystal structure. Table 4.2 shows standard d-spacing value and reflection plane indices (h, k, l) of magnetite (Fe_3O_4) structure.

Table 4.3 Measured d-spacing values of selected area in inner oxide layer formed under 5 m/s coolant velocity

Measured d-spacing	0.298	0.258	0.214	0.171	0.148	0.162
Standard d-spacing	0.298	0.254	0.209	0.171	0.148	0.160
(h, k, l)	2 2 0	3 1 1	4 0 0	4 2 2	4 4 0	5 1 1

The average d-spacing values of the selected area of the inner oxide are summarized in Table 4.3. The measured d-spacing values from the inner oxide layer clearly show that the inner oxide has Fe_3O_4 structure when compared with standard values of Fe_3O_4.

b) Outer Layer

Under 5 m/s coolant velocity, the outer oxide layer is composed of large octahedral crystals. The composition of the outer oxide is similar to the inner oxide, for iron and oxygen. The thickness of this layer was 0.22 micron.

Figure 4.7b shows the electron diffraction pattern of a selected area of outer oxide, indicated in Figure 4.7a. The average d-spacing values of the outer oxide are summarized in Table 4.4. It is seen that d-spacing values of the outer oxide are similar to standard values of Fe_3O_4.

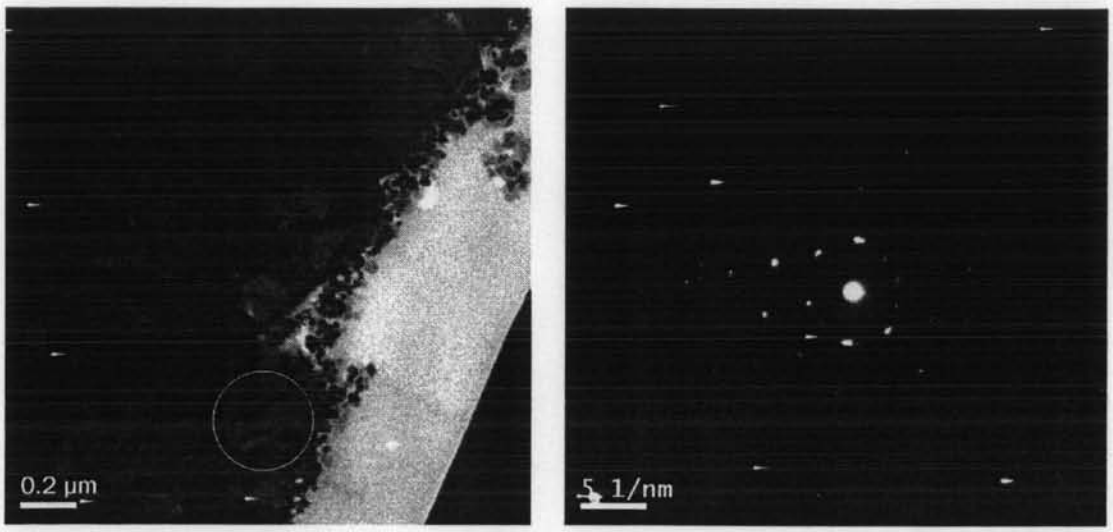

(a) (b)

Figure 4.7 TEM micrograph of outer oxide layer, which developed under 5 m/s coolant velocity, with its electron diffraction pattern.
(a) TEM micrograph of selected area in outer oxide layer. (b) Diffraction pattern of circular area.

Table 4.4 Measured d-spacing values of selected area in outer oxide layer formed under 5 m/s coolant velocity

Measured d-spacing	0.299	0.256	0.210	0.173	0.162
Standard d-spacing	0.298	0.254	0.209	0.171	0.160
(h, k, l)	2 2 0	3 1 1	4 0 0	4 2 2	5 1 1

TEM cross sectional analysis indicate that the oxide consists of a duplex layer, an inner layer and an outer layer. The outer layer was composed of large single octagonal particles while the inner layer consisted of well packed fine particles.

EDX mapping and depth profile investigated the chemical composition of the oxide. It was seen that the main components of both the inner and outer oxide were iron and oxygen. Moreover, the iron and oxygen ratio was relatively constant throughout the oxide. Therefore, both the inner and outer oxides

have the same molecular structure. The electron diffraction pattern indicated that the oxide was Fe_3O_4, regardless of particle size.

Cr, Si and Mn were detected in both the inner and outer layers. However, since their concentrations are very low, the effect of these compositions on oxide structure should be negligible.

4.1.2.2 10 m/s Coolant Velocity

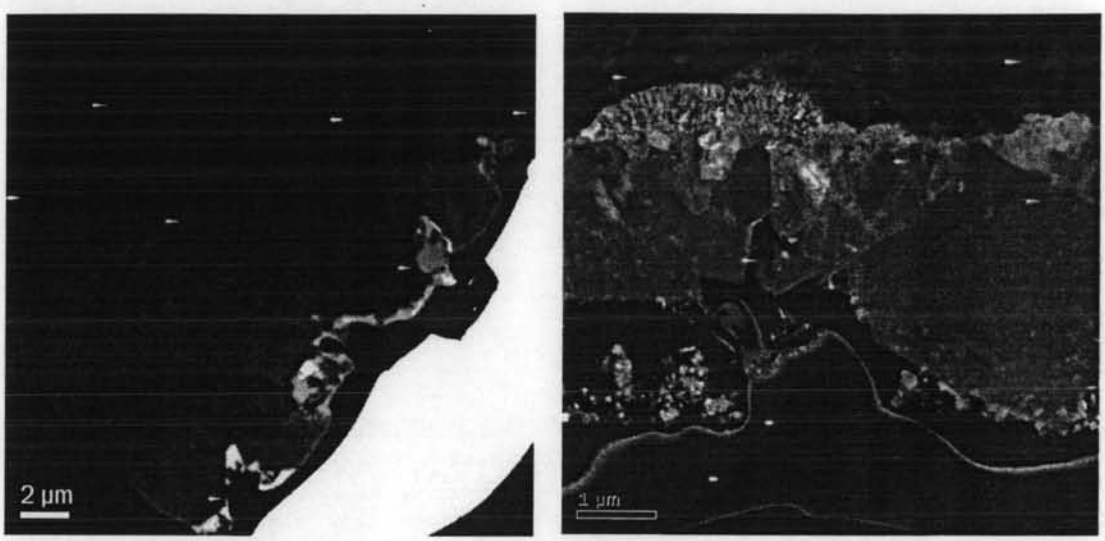

(a) Overview picture of oxide film (b) Oxide film in higher magnifications

Figure 4.8 TEM micrograph of oxide film formed under 10 m/s coolant velocity.

The Cross sectional micrograph of oxide film formed under 10 m/s coolant velocity is shown in Figure 4.8. The oxide layer has a rough surface due to variability in outer oxide size. It is surprising that these large oxide particles could not be observed by the SEM microscope. Therefore, the large particles must be covered by finer particles. Moreover, it is shown that there is a fluffy layer of fine particles which overlay the large particles. This phenomenon might be caused by the higher coolant flow velocity or different mechanism of formation. The inner oxide is uneven due to the original surface roughness.

Figure 4.9 shows the line scanning of the oxide layer which was formed under 10 m/s coolant velocity. The scanning was performed on 30 spots though out an oxide layer along the blue line, as shown in Figure 4.9a. The Fe and O

concentrations were analyzed along the blue line. From Figure 4.9b, the scanning shows a relatively constant Fe and O ratio. Therefore, both inner and outer oxides have the same structure. The reduction of Fe and O concentrations between the twenty-forth and twenty-seventh point is due to a cavity between the outer layer and a fluffy layer of fine particles. The Fe and O concentrations in the covering of fine particles have approximately the same concentrations as the inner and outer oxide. The Cr, Mn and Si content in the oxide is negligible.

Figure 4.10 shows EDX mapping of the oxide. The Fe and O maps show the transition boundary between metal and oxide. The O map confirms that both inner and outer layers consist of oxide compounds. The Mn map indicates the enrichment of Mn in the metal. The Si map shows enrichment of Si in the inner oxide.

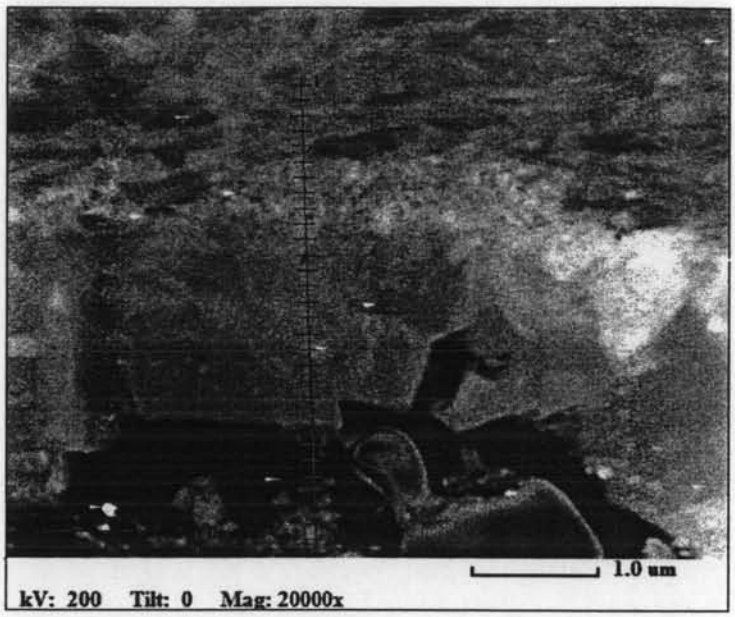

(a)

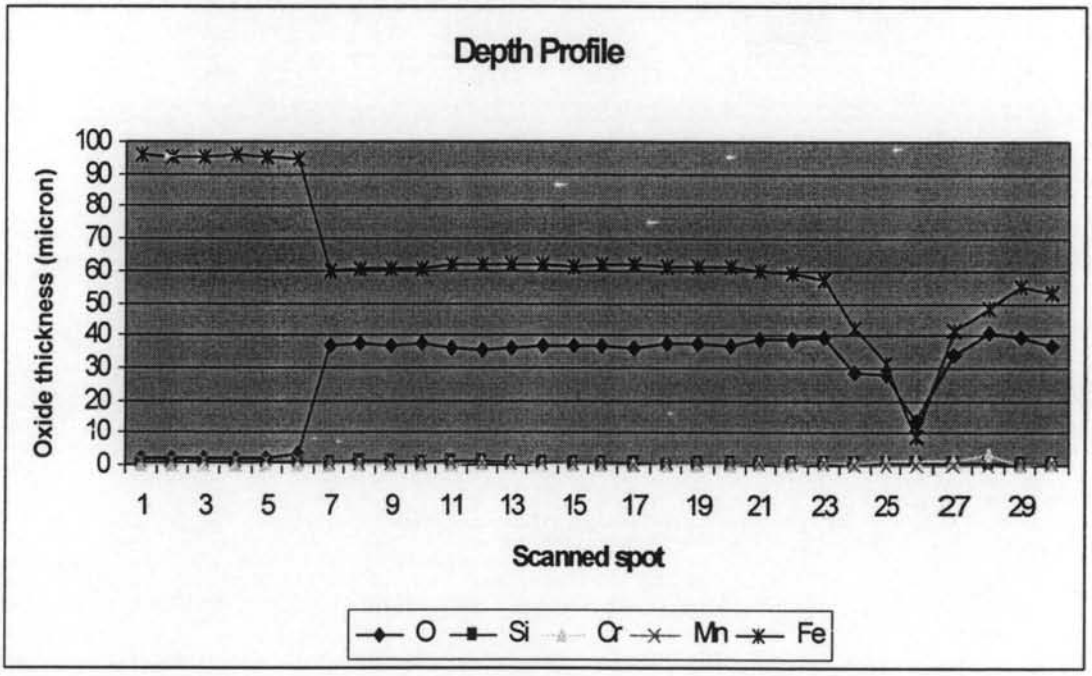

(b)

Figure 4.9 TEM line scanning of oxide film formed under 10 m/s coolant velocity. (a) TEM micrograph with annotated line. (b) Depth profile of oxide film.

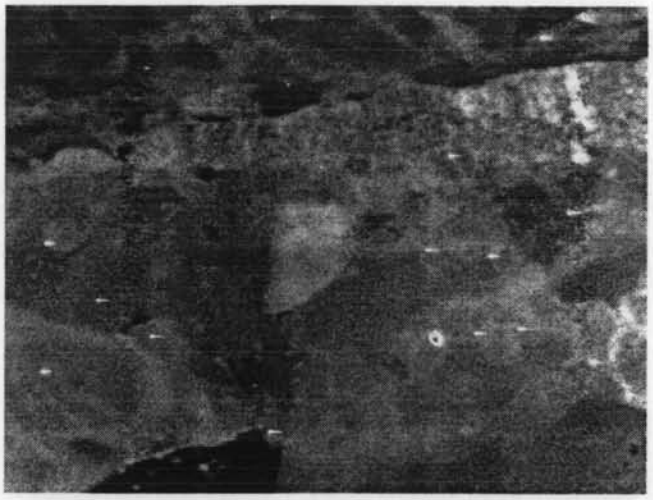

(a) Cross sectional micrograph of oxide film

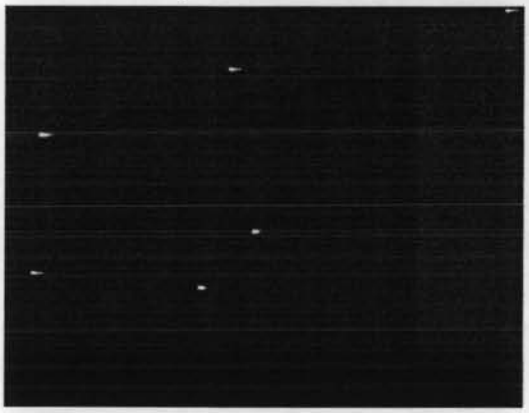

(a) Iron

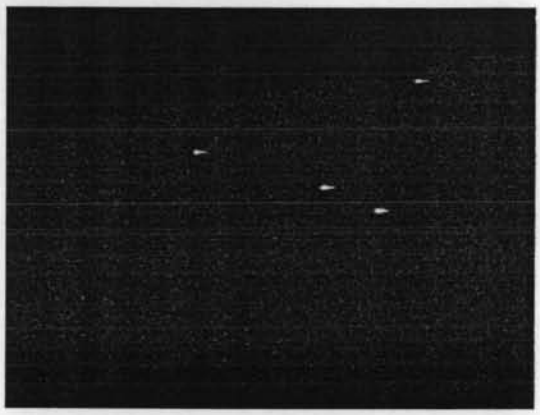

(b) Oxygen

(c) Manganese

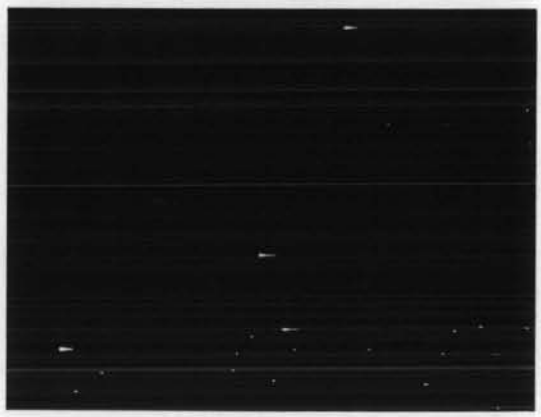

(d) Silicon

Figure 4.10 EDX mapping of 10 m/s sample.

a) Inner Layer

Since the original metal surface is rough, the inner oxide is uneven. The thickness of the inner oxide varied from less than 0.1 to 0.57 micron. The main composition of the oxide is iron and oxygen. The iron and oxygen concentrations in this layer are essentially constant at 60 % and 37 % respectively.

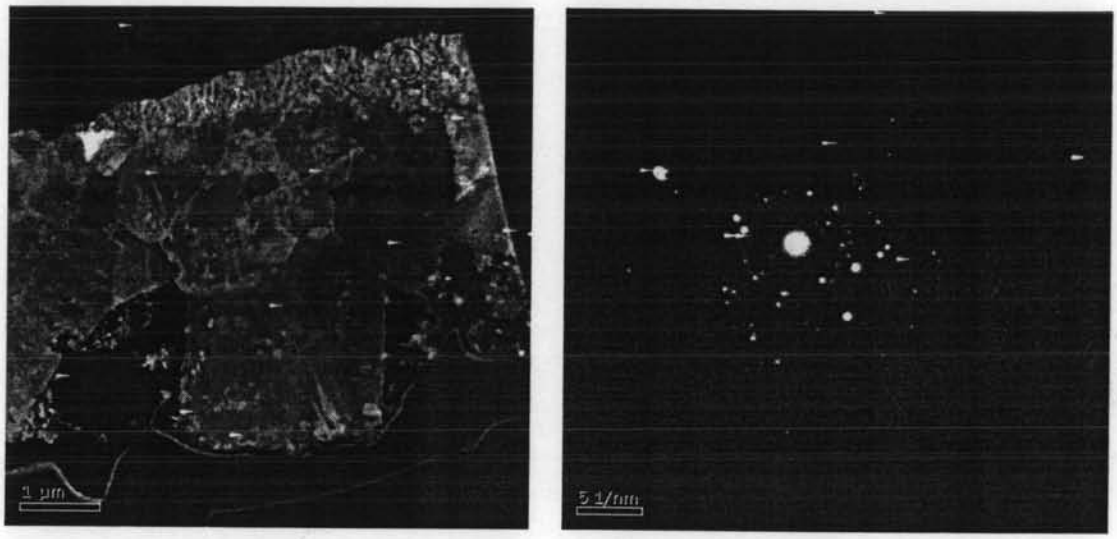

(a) (b)

Figure 4.11 TEM micrograph of inner oxide layer, which developed under 10 m/s coolant velocity, with its electron diffraction pattern.
(a) TEM micrograph of selected area in inner oxide layer. (b) Diffraction pattern of circular area.

To investigate the inner oxide structure, a selected area of the inner oxide was analyzed by electron diffraction pattern, as shown in Figure 4.11. A summery of d-spacing values which were measured from the selected area is shown in Table 4.5. The d-spacing values of the inner oxide agree with the standard values of Fe_3O_4.

Table 4.5 Measured d-spacing values of selected area in inner oxide layer formed under 10 m/s coolant velocity

Measured d-spacing	0.294	0.256	0.208	0.172	0.161
Standard d-spacing	0.298	0.254	0.209	0.171	0.160
(h, k, l)	2 2 0	3 1 1	4 0 0	4 2 2	5 1 1

b) Outer Layer

The outer oxide is composed of large single octahedral particles. Since the size of the outer oxide grain varies, the thickness of the outer oxide is between 0.79 and 4 microns. Moreover, under a 10 m/s coolant velocity, a fluffy layer of fine particles was observed over the outer oxide. The chemical compositions of the finer oxide, the outer oxide and the inner oxide are essentially the same. The iron and oxygen concentrations are 60 % and 37 % respectively.

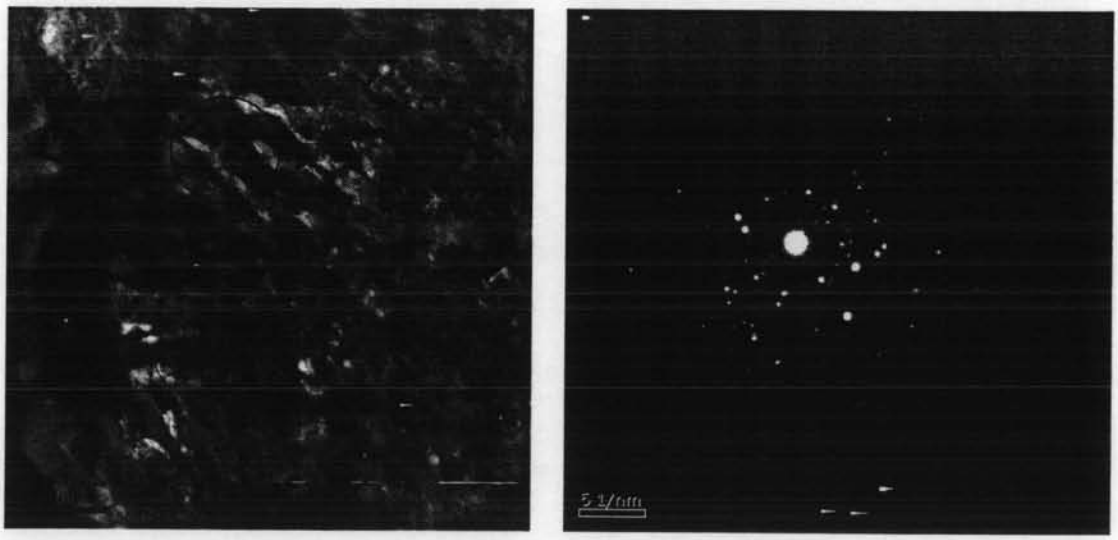

(a) (b)

Figure 4.12 TEM micrograph of outer oxide layer, which developed under 10 m/s coolant velocity, with its electron diffraction pattern.

(a) TEM micrograph of selected area in outer oxide layer. (b) Diffraction pattern of circular area.

Figure 4.12b shows the electron diffraction pattern of a selected area in the outer layer, as shown in Figure 4.12a. A summary of the average d-spacing values of the outer oxide are shown in Table 4.6. It is seen that the outer oxide d-spacing values are well matched with the standard values. Therefore, the outer oxide is Fe_3O_4.

Table 4.6 Measured d-spacing values of selected area in outer oxide layer formed under 10 m/s coolant velocity

Measured d-spacing	0.489	0.295	0.251	0.209	0.171	0.161
Standard d-spacing	0.485	0.298	0.254	0.209	0.171	0.160
(h, k, l)	1 1 1	2 2 0	3 1 1	4 0 0	4 2 2	5 1 1

The TEM cross sectional investigation reveals the large outer oxide particles although they could not be seen in the SEM micrograph, see Figure 4.2c. The large outer oxide particles were covered by a layer of finer particles. This fine oxide was also observed on the 20 m/s sample, as shown in Figure 4.4d. The finer oxide on the surface might come from the erosion of the outer oxide itself or a different mechanism of deposition.

EDX mapping and depth profiles show that the chemical concentration of the inner oxide, outer oxide and the covering of fine particles are similar. The electron diffraction pattern indicated that they had the same structure, Fe_3O_4.

Traces of other components, such as Cr, Mn and Si, were detected by EDX. However, their concentrations are very low. Therefore, their effect on the oxide structure is negligible.

4.1.2.3 20 m/s Coolant Velocity

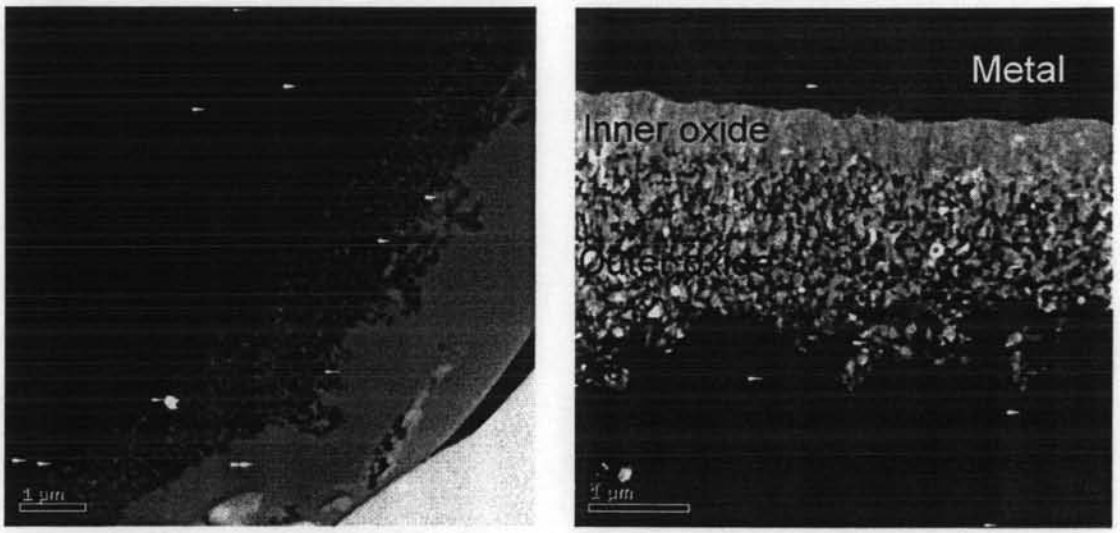

(a) Overview picture of oxide film (b) Oxide film in higher magnifications

Figure 4.13 TEM micrograph of oxide film formed under 10 m/s coolant velocity.

A duplex oxide layer was formed under 20 m/s coolant velocity, as shown in Figure 4.13. Apparently, the inner oxide, which has smaller particle size, has denser packing than the outer oxide.

Figure 4.14 shows a line scanning on the oxide film. The fluctuation of Fe and O concentrations in the outer oxide confirms the loose packing of particles. Traces of contamination elements could be detected in the oxide. However, these elements are at very low concentrations.

Figure 4.15 shows an EDX mapping of the oxide. The iron and oxygen maps clearly indicate the metal/oxide interface. The O map confirms that both inner and outer layers consist of an oxide compound. The Cr map indicates Cr in both the inner and outer oxide. The Ni map shows a contamination of Ni in the oxide film. The higher values in the outer oxide layer, Ni is not contained in A106B steel, indicate that the contamination must come from the loop. Figure 4.15e shows that Ni did not diffuse to oxide/metal interface and was blocked by the inner oxide layer.

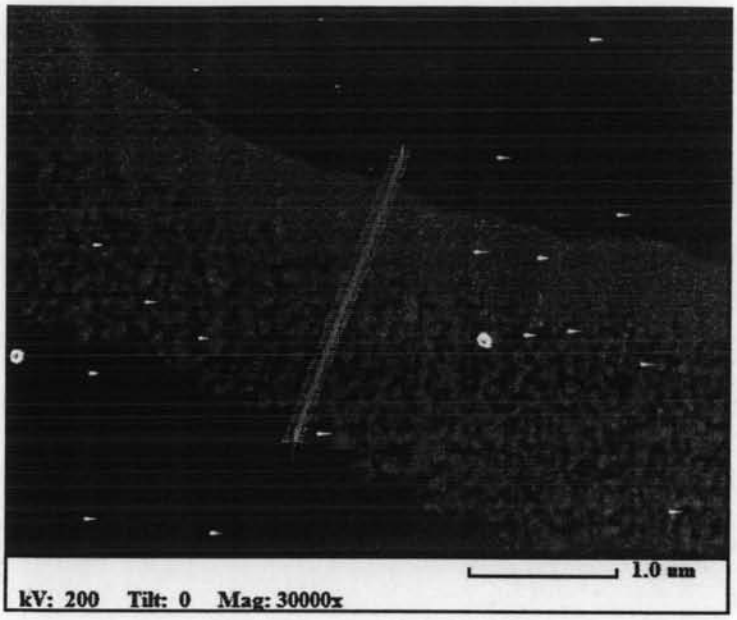

(a)

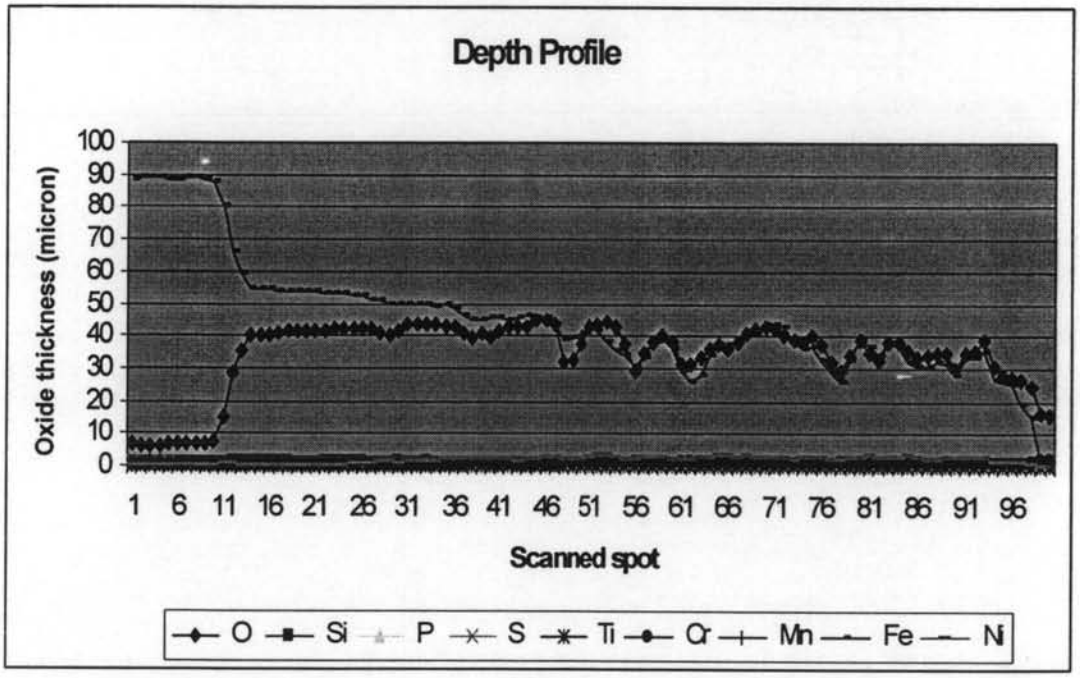

(b)

Figure 4.14 TEM line scanning of oxide film formed under 10 m/s coolant velocity. (a) TEM micrograph with annotated line. (b) Depth profile of oxide film.

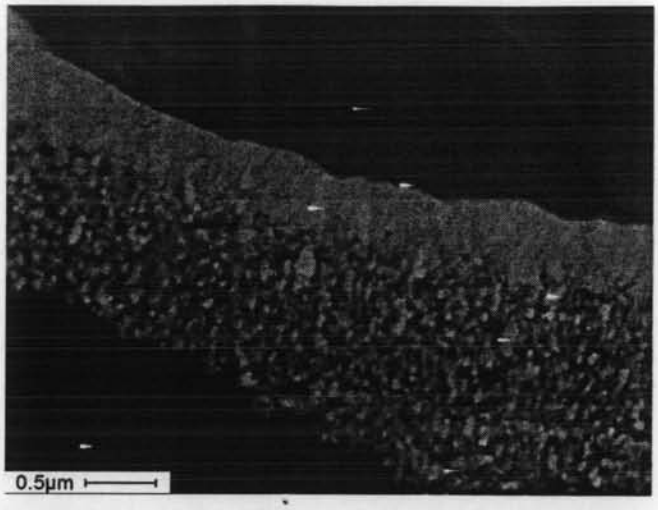

(a) Cross sectional micrograph of oxide film

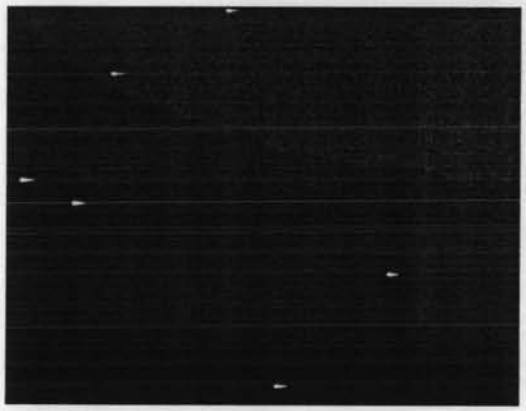

(b) Iron

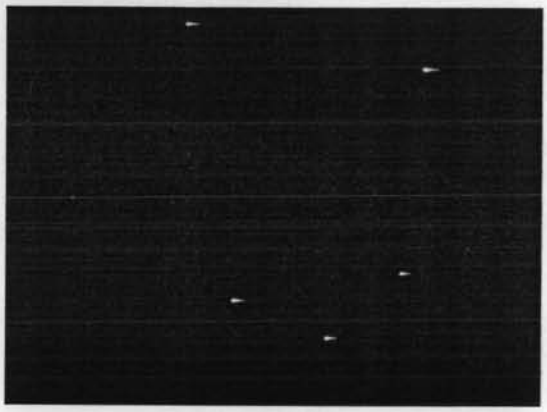

(c) Oxygen

(d) Chromium

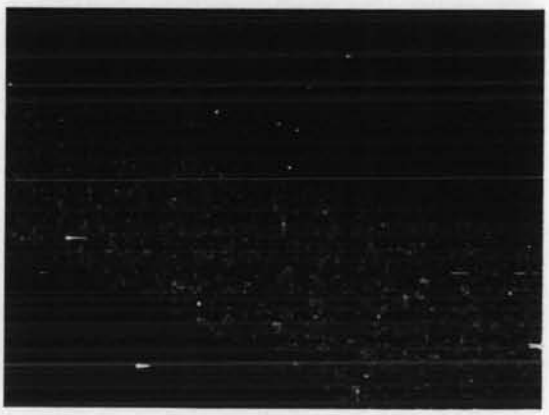

(e) Nickel

Figure 4.15 EDX mapping of 20 m/s sample.

a) Inner Layer

The inner oxide layer consists of small oxide particles with highly dense packing. The main compositions are iron and oxygen. The iron and oxygen concentrations in this layer are constant at 50 % and 43 % respectively. The thickness of this layer is 0.56 microns.

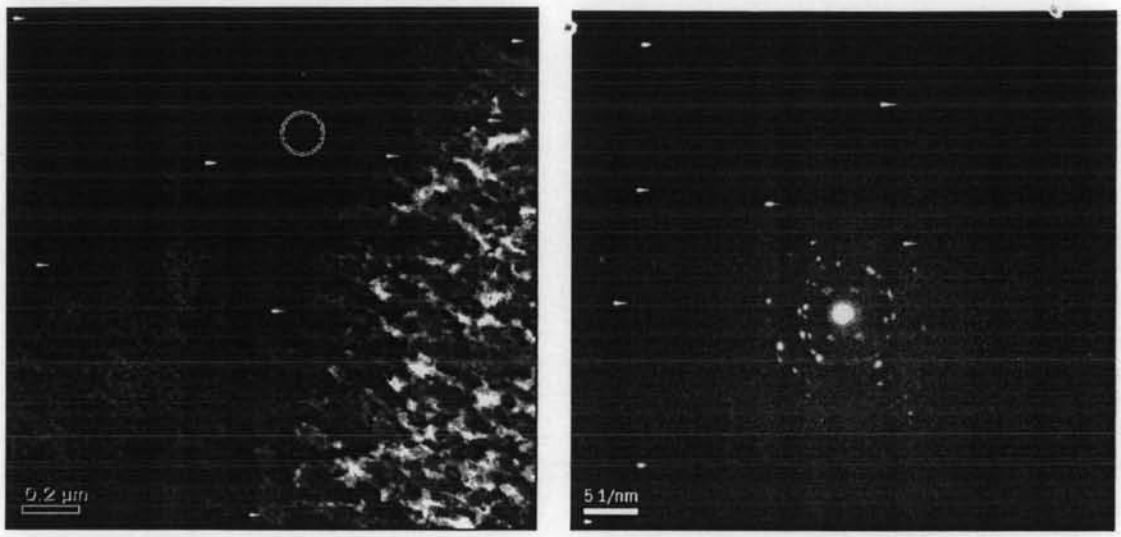

(a) (b)

Figure 4.16 TEM micrograph of inner oxide layer, which developed under 20 m/s coolant velocity, with its electron diffraction pattern.
(a) TEM micrograph of selected area in inner oxide layer. (b) Diffraction pattern of circular area.

Figure 4.16b shows the electron diffraction pattern of a selected area in the inner oxide, as indicated in Figure 4.16a. The d-spacing values of the inner oxide are summarized in Table 4.7. The measured d-spacing values indicated that the inner oxide has Fe_3O_4 structure.

Table 4.7 Measured d-spacing values of selected area in inner oxide formed under 20 m/s coolant velocity

Measured d-spacing	0.494	0.301	0.257	0.216	0.175	0.165	0.151
Standard d-spacing	0.485	0.298	0.254	0.209	0.171	0.160	0.148
(h, k, l)	1 1 1	2 2 0	3 1 1	4 0 0	4 2 2	5 1 1	4 4 0

b) Outer Layer

Under 20 m/s coolant velocity, the outer oxide layer is composed of a loose packing of large single octahedral oxide. The film thickness is 1.25 microns. The outer oxide is mainly composed of iron and oxygen. Iron and oxygen concentration in this layer fluctuated due to the loose packing of oxide particles, as shown in Figure 4.14b. However, the average concentrations are essentially the same as the inner layer.

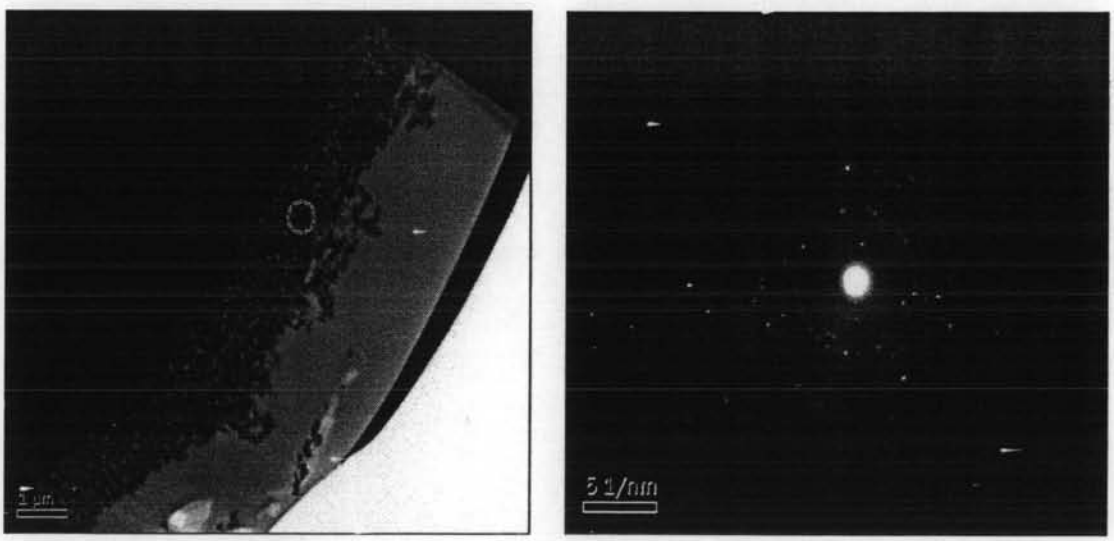

(a) (b)

Figure 4.17 TEM micrograph of outer oxide layer, which developed under 20 m/s coolant velocity, with its electron diffraction pattern.
(a) TEM micrograph of selected area in inner oxide layer. (b) Diffraction pattern of circular area.

Figure 4.17b shows the electron diffraction pattern of a selected area in the inner oxide, as indicated in Figure 4.17a. A summary of d-spacing values measured from the outer oxide are shown in Table 4.8. It is clear that the outer oxide is Fe_3O_4.

Table 4.8 Measured d-spacing values of selected area in outer oxide formed under 20 m/s coolant velocity

Measured d-spacing	0.487	0.295	0.254	0.249	0.210	0.172	0.162
Standard d-spacing	0.485	0.298	0.243	0.254	0.209	0.171	0.160
(h, k, l)	1 1 1	2 2 0	2 2 2	3 1 1	4 0 0	4 2 2	5 1 1

TEM cross sectional analysis indicates that the duplex oxide which developed under 20 m/s coolant velocity has different packing densities. The oxide particle size is essentially uniform at 1 micron.

EDX mapping and depth profiles indicated the chemical compositions of the oxide. Although there was fluctuation of iron and oxygen concentrations in the outer oxide, the average concentrations were similar. The fluctuation was caused by the loose outer oxide packing. However, electron diffraction patterns confirm that both the inner and outer oxides have similar structure, Fe_3O_4.

From TEM cross sectional investigation, it is clearly seen that the oxide film consist of two layers with different characteristic, an inner layer with fine oxide grain and an outer layer of large oxide crystals. Thicknesses of the inner and outer oxide layers at each velocity are shown in Table 4.9.

Table 4.9 Oxide thickness formed in each coolant velocity

Coolant velocity (m/s)	Oxide thickness (micron)	
	Inner layer	Outer layer
5	0.08-0.74	0.22
10	0.1-0.57	0.79-4
20	0.56	1.25

It was found that the oxide formed at 10 m/s velocity has the thickest inner and outer oxide layer, which agrees with SEM results. However, these results contradict the assumption that the thickest oxide would be expected of 5 m/s due to less shear stress. It is possible that the oxide formed at the 5 m/s velocity required more time to reach its steady state. Additional experiments are required to determine the length of time to reach steady state.

There are some fine particles observed on the outer oxide layer formed at high velocities, especially in the 10 m/s sample. EDX analysis indicated that these particles have the same composition with the inner and outer oxides. Therefore, it is possible that these fine particles are a product from erosion of the outer oxide due to the coolant flow or a different mechanism of deposition. It appears that flow velocity has a significant effect on the outer oxide structure.

EDX and depth profiles indicated that all the inner and outer oxides have a similar composition, regardless of flow velocity. Electron diffraction patterns indicated that all the inner and outer oxide is Fe_3O_4, regardless of flow velocity. However, in the 20 m/s sample, there is high Ni concentration in the oxide particles, especially in outer oxide layer. This might affect the molecular structure of oxide particles.

The general formula of the spinel structure is AB_2O_4, where A is a cation with +2 charge and B is a cation with +3 charge. The general structure of magnetite (Fe_3O_4) is $Fe^{2+}O.Fe^{3+}{}_2O_3$. Ni^{2+} can substitute in Fe^{2+} positions because their charge and ionic radii are similar. Therefore, if there is significant Ni contamination in the system, the oxide structure could be either magnetite (Fe_3O_4) or nickel ferrite ($NiFe_2O_4$). Moreover, the d-spacing values of these compounds are similar as well. Therefore, it is difficult to distinguish the oxide structure by the electron diffraction pattern.

The oxide microstructure can be identified by the spinel stoichiometry. The stoichiometry of a spinel structure $(Ni_xFe_{3-x})O_4$ indicates that the inner and outer oxides formed under 20 m/s velocity are $Ni_{0.15}Fe_{2.85}O_4$ and $Ni_{0.55}Fe_{2.45}O_4$, respectively.

Cr^{3+} can substitute Fe^{3+} positions in the spinel structure. However, the Cr concentration in the oxide is very low (less than 1 %). Therefore, its effect on the molecular structure of the oxide may not be significant for A106B steel.

Traces of other components were detected by EDX. However, their concentrations are very low. Therefore, their effect on the oxide structure is believed to be negligible.

4.2 Wall Shear Stress Simulation

The wall shear stress of an outlet feeder, S08, in a CANDU reactor was simulated by Fluent. The shear stress distribution on the S08 pipe is shown in Figure 4.18. The red shade area represents high local shear stress while the blue shades area represents low local shear stress. It is seen that high shear stress is found at next to the end of extrados and spreads out through the right side of feeder (looking down stream). For the intrados, the local shear stress is relatively low. Low shear stress was also found around the intrados of feeder and to the left of the pipe (looking down stream).

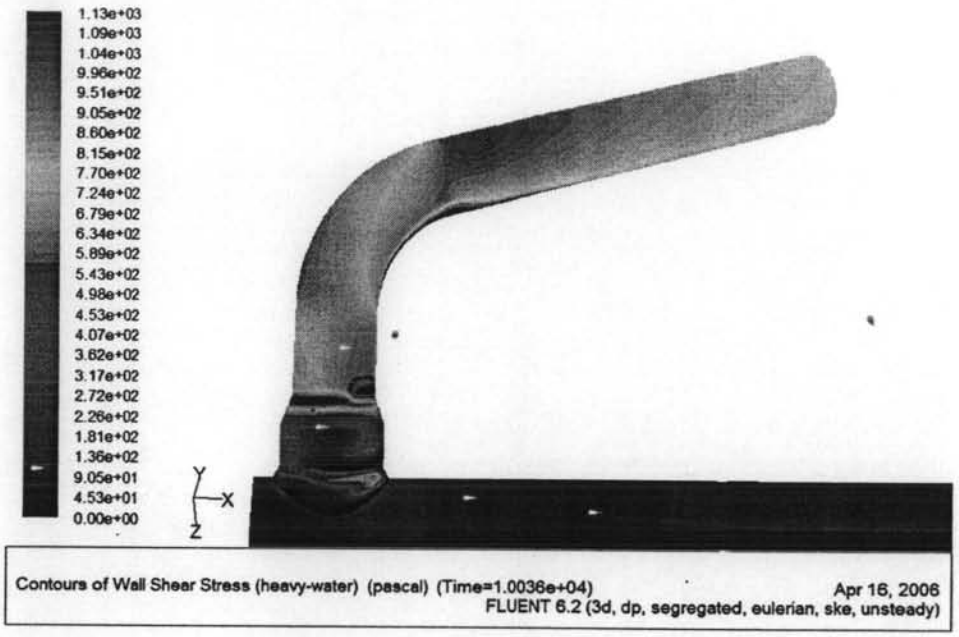
1.13e+03
1.09e+03
1.04e+03
9.96e+02
9.51e+02
9.05e+02
8.60e+02
8.15e+02
7.70e+02
7.24e+02
6.79e+02
6.34e+02
5.89e+02
5.43e+02
4.98e+02
4.53e+02
4.07e+02
3.62e+02
3.17e+02
2.72e+02
2.26e+02
1.81e+02
1.36e+02
9.05e+01
4.53e+01
0.00e+00
Y
X
Z
Contours of Wall Shear Stress (heavy-water) (pascal) (Time=1.0036e+04)
Apr 16, 2006
FLUENT 6.2 (3d, dp, segregated, eulerian, ske, unsteady)

(a)

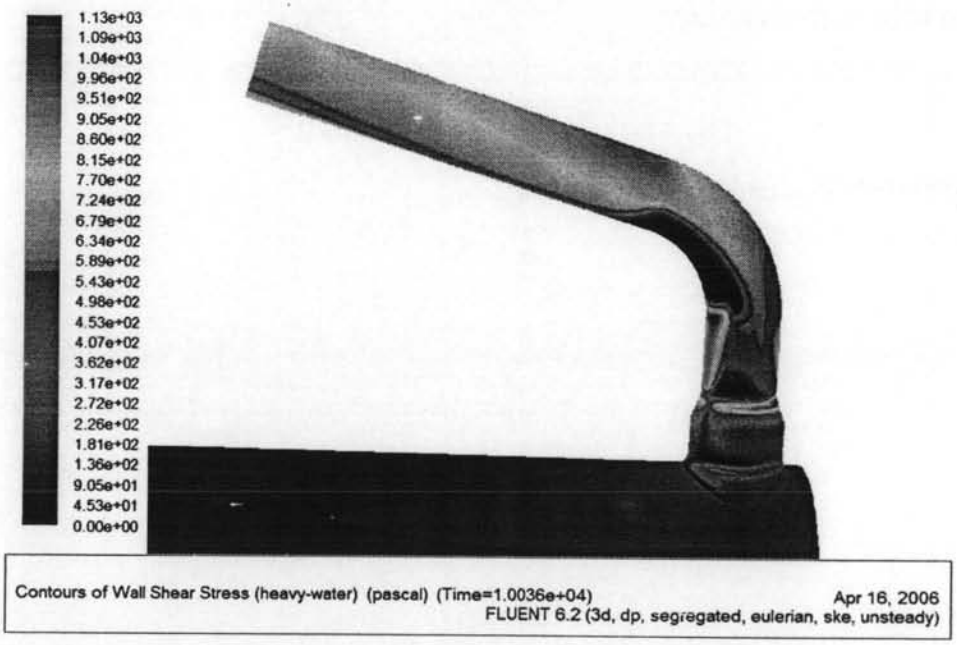
1.13e+03
1.09e+03
1.04e+03
9.96e+02
9.51e+02
9.05e+02
8.60e+02
8.15e+02
7.70e+02
7.24e+02
6.79e+02
6.34e+02
5.89e+02
5.43e+02
4.98e+02
4.53e+02
4.07e+02
3.62e+02
3.17e+02
2.72e+02
2.26e+02
1.81e+02
1.36e+02
9.05e+01
4.53e+01
0.00e+00
Contours of Wall Shear Stress (heavy-water) (pascal) (Time=1.0036e+04)
Apr 16, 2006
FLUENT 6.2 (3d, dp, segregated, eulerian, ske, unsteady)

(b)

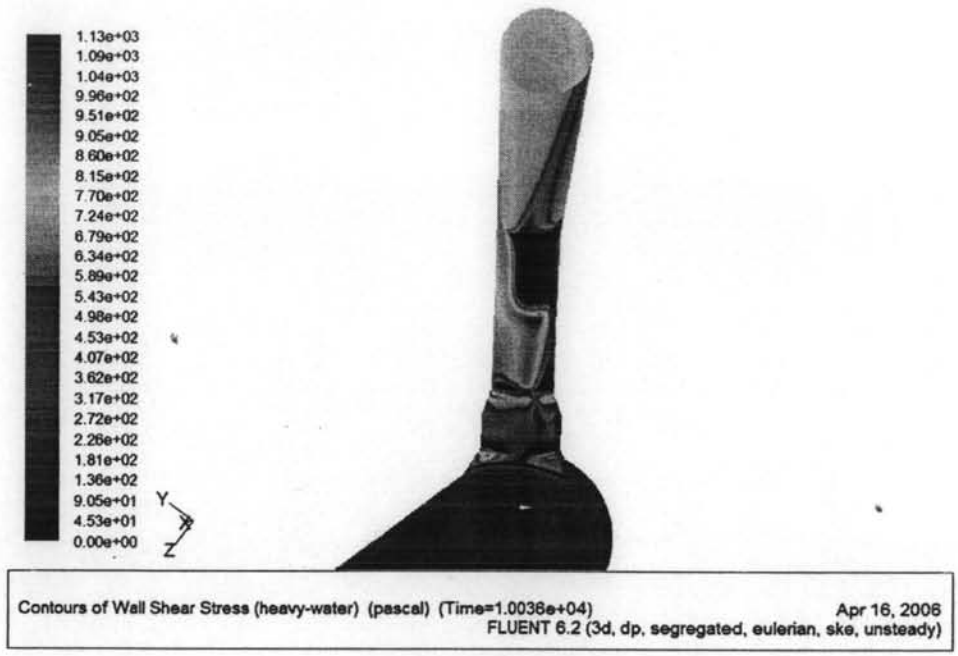

(c)

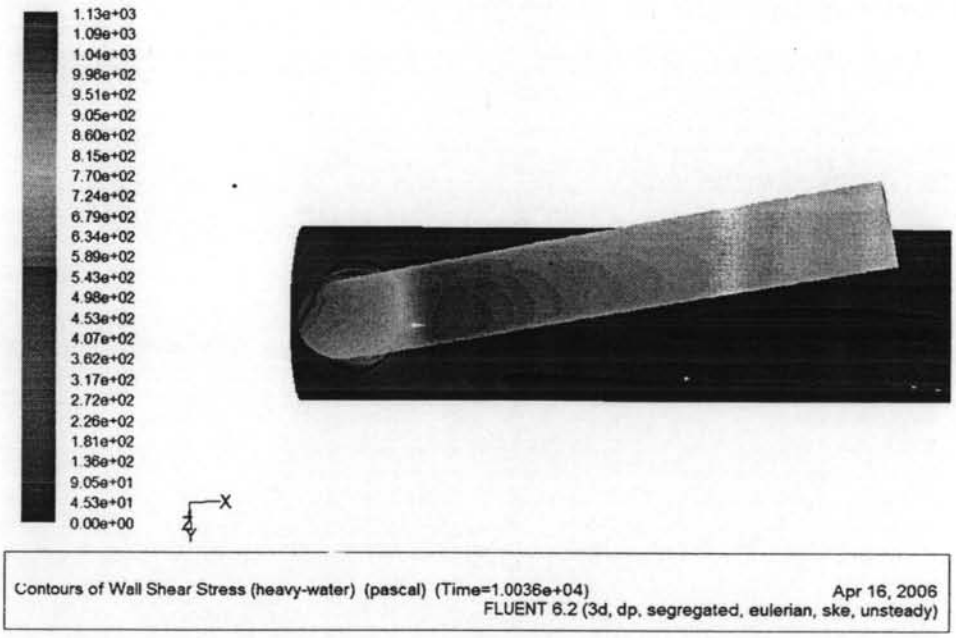

(d)

Figure 4.18 Simulated wall shear stress distributions on S08 outlet feeder.

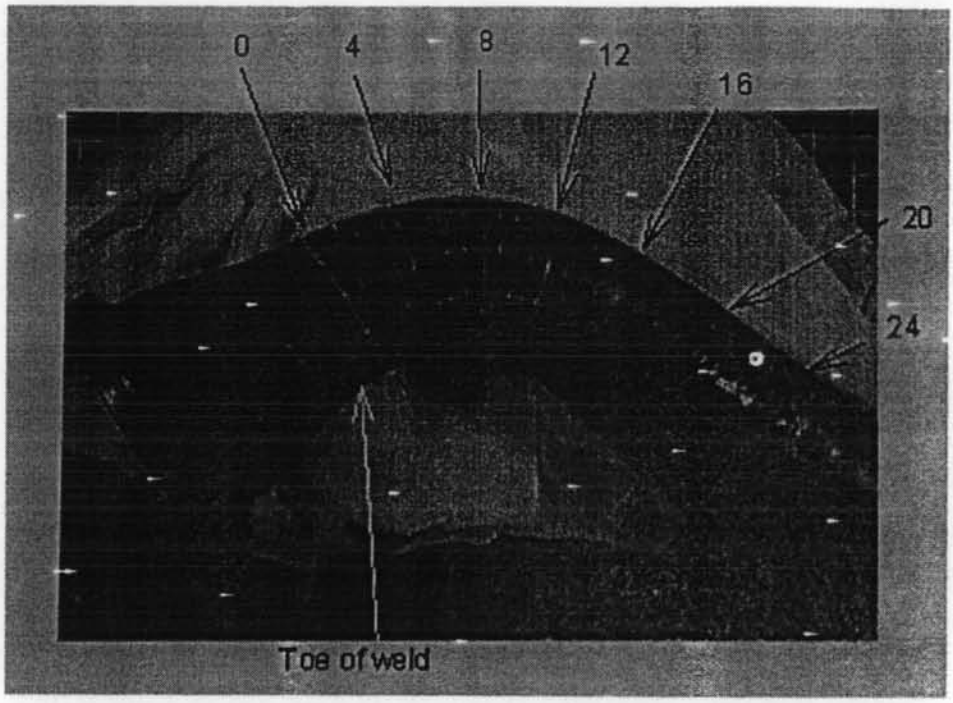

Figure 4.19 S08 outlet feeder pipe in CANDU reactor.

The oxide thicknesses of the S08 pipe removed from the CANDU reactor at Point Lepreau were measured at various distances and angles. The S08 pipe and the annotated line are shown in Figure 4.19. The reference 12.00 o'clock position is taken as the line along the extrados of bend. The oxide thicknesses measured from SEM micrographs and the average local shear stress are shown in Table 4.10.

Table 4.10 The oxide thickness measured from S08 pipe in Point Lepreau

Sample	Clock position	Axial length from weld toe (cm)	Circumference line	Oxide thickness (microns)	Local shear stress (Pa)
E4G	0:30	3.33	2	1.36	599.84
E3F	0:30	7.81	7	1.30	622.48
E3J	0:30	10.91	10	1.37	622.48
E4D	3:30	3.25	4	1.16	735.66
E4A	5:30	3.20	5	1.03	894.11
E2C	5:30	5.25	9	1.39	622.48
E2F	5:30	7.14	13	3.05	11.32
F2A7	6:30	7.14	13	2.82	11.32
F2A4	8:30	9.04	12	1.85	282.94
F2A1	11:30	10.91	10	1.62	577.21

Table 4.8 states that the oxides along the extrados, 0.30 o'clock, are relatively constant while it becomes thinner at the right side of feeder, 3.30 o'clock. At the beginning of intrados, slightly to the right, 5.30 o'clock, the oxide is quite thin; however, the oxide becomes thicker at further intrados points. From Figure 4.18b, the oxide in the blue shade area, 8.30 o'clock, is relatively thicker than the oxide on extrados. Figure 4.18d shows that local shear stress in 11.30 o'clock is slightly less than the shear stress at 0.30 o'clock which corresponds to the oxide thickness data from the plant. The relation between the oxide thickness and the local shear stress are shown in Figure 4.20. Most of the results indicate that the oxide has a thin layer in high shear stress areas and a thick layer in low shear stress areas.

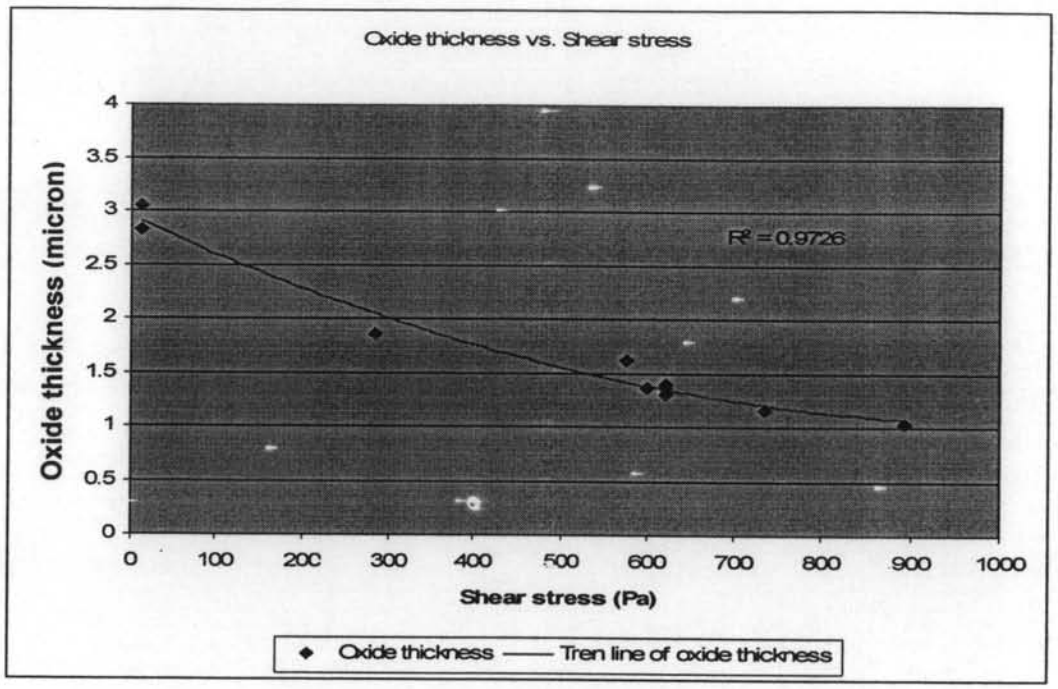

Figure 4.20 The relations between oxide thickness and the local shear stress.

Supa-Amornkul (2000) studied relationship between the experimental metal loss rate and shear stress, as shown in Figure 4.21. The data labeled "UT" indicated ultrasonic probe and the non-labeled data indicated the data form wire resistance probes.

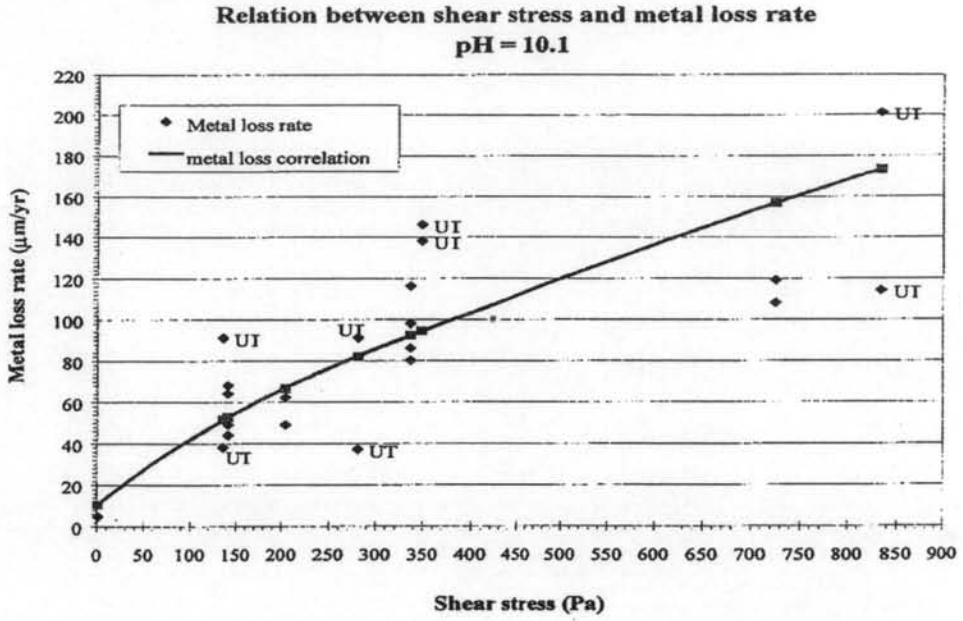

Figure 4.21 Relationship of metal loss rate and shear stress.

From the data, the correlation between the metal loss rate and the shear stress was derived as:

$$m = 7.65\ (1+0.111\tau^{0.75})(1+1.51 \times 10^{-9}\ e^{1.87pH}) \qquad (4.1)$$

m = corrosion rate (micron/yr)

τ = Shear stress (Pa)

The calculated shear stress from this equation gave the corresponded values for the data from F11 outlet feeder pipe in CANDU reactor (Supa-Amornkul, 2000). The equation indicated that the corrosion rate depends upon the shear stress to the power of 0.75 and the exponential of pH. The metal loss rate increases as the shear stress increases. In addition, the oxide thickness decreased when the shear stress increases. Therefore, a thin oxide film trends to promote high corrosion rates.